The 1.5-5-day Eastward Waves in the Upper Stratosphere-Mesosphere as Observed by the Esrange Meteor Radar and the SABER Instrument

E.G. Merzlyakov[1*] and D.V. Pancheva[2]

[1] Institute for Experimental Meteorology, Obninsk, Russia
[2] Dept. of Electronic & Engineering, University of Bath, Bath, UK

* Corresponding author: E. Merzlyakov, e-mail: eugmer@typhoon.obninsk.ru
Institute for Experimental Meteorology, Lenin Str. 82, Obninsk, Kaluga reg., 249038, Russia

Key words: polar vortex, wave-wave interaction, jet instability, Eliassen-Palm flux, stratosphere-mesosphere coupling

Abstract: Data of neutral meridional wind obtained by the meteor radar at Esrange and data of temperature and pressure measured by the Sounding of the Atmosphere using Broadband Emission Radiometry (SABER) instrument on board the Thermosphere–Ionosphere–Mesosphere Energetics and Dynamics (TIMED) spacecraft were studied with respect to a day-to-day atmospheric variability with periods from 1.5 to 5 days. The detailed analysis was carried out for February 2004. Perturbations of the atmospheric parameters at the examined periods appeared mainly as eastward propagating waves of zonal wavenumbers 1 and 2. We suggested that these waves excited by the jet instability on both flanks of the polar night jet in the upper stratosphere and mesosphere interact non-linearly with each other, and this interaction generates secondary waves. The radar observed both primary and secondary waves at mesospheric heights. The data analysis supports this suggestion. Under conditions of weaker instability observed in February 2003 the perturbations of atmospheric parameters of periods from 1.5 to 5 days had smaller amplitudes at heights of the mesosphere than those in February 2004. It was found that the Eliassen-Palm fluxes calculated for the waves generated by the jet instability were mainly downward directed. This result suggests a possible dynamical influence of the mesospheric layers on the lower atmospheric levels.

1. Introduction

The eastward propagating 4-day wave is a characteristic feature of the winter stratosphere in both hemispheres. Initially it was observed in temperature by Venne and Stanford (1979; 1982) with the Nimbus-5 Selective Chopper Radiometer. Further investigations have shown that simultaneously there exist waves with zonal wave number *s* in a range from 1 through 4 in different atmospheric parameters. The waves propagate with close phase velocities, or as a wave packet, so that the s=1 wave has a period of 4 days, while the s=2 wave has a period of 2 days and so on. It was suggested that a source of the observed oscillations is the baroclinic/barotropic instability of the winter polar jet (Hartmann, 1983; Manney and Randel, 1993; Lawrence and Randel, 1996). Allen et al. (1997) applied a concept of the potential vorticity "charge". The charge generated by the instability introduces anomalies in temperature, pressure, wind and particularly in ozone. Coy et al. (2003) considered the polar 2-day wavenumber-2 component of the 4-day wave event and showed that the 2-day wave represented the major source of the ozone variation in July 1998 at 70^0S.

Meteor (MR) and medium frequency (MF) radars provide practically continuous hourly mean wind measurements in the mesosphere/lower thermosphere (MLT) at heights from 70 km to 110 km. Only few studies have examined a connection between wind oscillations in the MLT region and in the upper stratosphere. For example, Lawrence et al. (1995) investigated the 4-day wave in the Antarctic winter mesosphere using radar wind measurements and results of the stratospheric analysis and demonstrated correlation between stratospheric and mesospheric events. The way in which the waves penetrate from the stratosphere into the mesosphere was left unclear. Lawrence et al. (1996) analyzed geopotential data from the Pressure Modulated Radiometer data (aboard Nimbus 6) and found the 4-day s=1 wave throughout the altitude range 30-90 km in the Southern hemisphere. That points out a possible direct connection between the 4-day events in the MLT and stratosphere.

A strong winter quasi-two-day wave (QTDW) in the neutral wind has been found recently. It appears regularly in the MLT of the Northern hemisphere during winter and has amplitudes larger than its summer counterpart (Nozawa et al., 2003). Merzlyakov et al. (2005) showed that the simultaneous wind measurements at Dixon Island. (80^0E, 72.5^0N) and Esrange (21^0E, 68^0N) gave evidence for a strong eastward propagating QTDW in the winters of 1999/00 and 2000/01. The estimated zonal wavenumber for those waves was 2. Additionally an s=1 wave with a period of about 5 days was observed. Of course, with just two stations, wavenumbers cannot be resolved unambiguously. We presume that the eastward propagating waves observed in the stratosphere and in the MLT region are of the same primary origin and this is actually the main subject of this work.

In this study we use the temperature and pressure dataset obtained from the measurements by the Sounding of the Atmosphere using Broadband Emission Radiometry (SABER) instrument onboard the Thermosphere–Ionosphere–Mesosphere Energetics and Dynamics (TIMED) spacecraft and data of coincident measurements of wind carried out by the MR at Esrange. Our preliminary investigation of the available data (years 2003-2004) for the Arctic winter months indicated that the strongest 2-4 day waves existed in February 2004. A major stratospheric warming happened in early January 2004. It led to a long lasting (nearly 2 months) vortex disruption in the middle and lower stratosphere. The upper stratospheric vortex broke up in late December, but began to recover in early January, and then it strengthened significantly in February (Manney et al., 2005). Venne and Stanford (1982) observed a coincidence of major and final warmings with decreases in the 4-day amplitudes. The presence of the strong 4-day wave in temperature during February 2004 has already been reported by Garcia et al. (2005).

We analyze perturbations of atmospheric parameters with periods ranging from 1.5 days to 5 days. Our main goal is to reveal the sources of the wind variations observed by the radar and to correlate results of wind measurements in the MLT with the temperature and pressure perturbations obtained from measurements of the SABER instrument in the upper stratosphere and mesosphere. First, we demonstrate similarity between MLT wind oscillations measured by the radar and the wind

oscillations calculated from coincident stratosphere-mesosphere oscillations in pressure and temperature observed by SABER in February 2004. Then, we analyze these oscillations in detail and show that their features indicate that both the jet instability and the nonlinear wave-wave interaction are the forcing mechanisms of these waves. At the end, we present some results for February 2003 to compare perturbations of atmospheric parameters during winters with polar vortex of different strength.

2. Data analysis

We use hourly mean neutral wind data obtained by the MR radar at Esrange during February 2003 and 2004. The results for the meridional wind component are mainly presented in this study. There are two reasons for this: (i) this wind component has a simple latitude-height structure similar to that of the pressure field (primary reason), and (ii) it can be determined from the pressure oscillations with smaller errors than those of the zonal wind component (secondary reason). Wavelet analysis and periodogram analysis have been used to analyze features of the 1.5-5-day oscillations in the MLT wind.

The SABER data are the "Level 2A" data, which were available online as the data of version 1.06 at http://saber.larc.nasa.gov. SABER is a 10-channel radiometer that measures the infrared radiation from the Earth's limb from the surface to the lower thermosphere every 58 s with ~2-km vertical resolution (a detailed explanation see, for example, Russell et al., 1999).

The SABER data were processed onto a regular height-latitude grid between 30km and 100km in height and between 35^0N and 75^0N in latitude with steps of 5 km and 5^0, respectively. We constructed in advance monthly mean zonal mean temperature, pressure (P) and density (ρ_0) distributions by gridding the SABER measurements for the entire month and then calculating the zonal means. Then, the SABER data were rearranged into data rows of ascending and descending soundings. These rows are averaged for neighboring orbits which intersect a given cell of the grid in correspondence with time and longitude. The averaging region has a center located at the grid point and dimensions of 3 km (in height) and 5^0 (in latitude). In this way we obtained rows of average values of temperature and pressure/ρ_0 which are practically equidistant in time and in longitude in accordance with the intersections of the fixed latitudinal circle by the satellite (errors of steps are stochastic with r.m.s. deviation less than 0.6% for time points and ranging from 0.6% to 10% for longitudes, where a strong increase of the error is valid for latitudes, higher than 70^0N). The method of asynoptic sampling described by Salby (1982) with the modification proposed by Lait and Stanford (1988) was used to perform spectral analysis on the rows of ascending and descending data. The errors in distance between points are ignored and the points are taken with the average distance between them. As it was checked and pointed out by Lait and Stanford (1988) the errors mentioned above did not practically influence the results. Our tests confirmed this finding. We found that the errors of the spectral peaks depend on the spectrum of the data analyzed. In our case the errors of the spectral peaks presented in this work are less than 3%. For larger peaks corresponding, for example, to stationary planetary wave 1 -3, or the diurnal migrating tide the errors are less than 1%.

There are two popular ways to determine a statistical significance of spectral distributions; see for example Mechoso and Hartmann (1982). We employ the calculation of coherence between rows at the peak of amplitude and elsewhere. The number of degrees of freedom is 9.2. In this case a coherence level of 0.55 corresponds to the 95% confidence level.

Spectra of the horizontal wind velocities were calculated from the spectral distributions of the pressure oscillations. In order to do this we assumed that: (i) external sources of momentum are absent, and (ii) vertical wind can be ignored, (iii) diffusion is ignored as well. We employed for our calculation linear balance equations taking into account the background zonal mean zonal wind. The validation of this approach and shortcomings are discussed in Appendix. The approach is

similar to that one used by Lawrence and Randel (1996). Our calculations included the pressure oscillations of only zonal wavenumbers from -3 to 3. Indeed, only eastward propagating waves had the large amplitudes and coherent parameter distributions, while westward propagating waves provide mainly noise. For periods ranging from 1.5 days to 5 days and wavenumbers from -3 to 3, 80% of the variance is due to eastward propagating waves. This value is about 70% if one takes into account all wavenumbers (up to 7).

To detect the wave sources and to estimate the influence of the waves studied in this work on zonal mean circulation we calculated divergence of Eliassen-Palm (EP) flux (Andrews, 1987). Our numerical simulations (see Appendix) demonstrated that there is no principal difference between the distribution of the EP flux divergence for waves forced by the jet instability and by the nonlinear wave-wave interaction. However, these numerical runs showed that the nonlinear interaction is actually a weak wave source in comparison with the instability. As a result of this the maxima of the EP flux divergence and convergence for primary waves were greater by about one order of magnitude than those of the secondary waves forced by the nonlinear interaction. On the other hand we numerically obtained that the polar night jet should be unstable in February 2004 (see Appendix) and the most prominent perturbations of atmospheric parameters can be attributed to waves generated by the polar jet instability.

On the basis of the above mentioned numerical results one can propose the following interpretation of the wind variability studied in this work: the instability of polar night jet is a source of the primary most prominent waves, these primary waves non-linearly interact with each other and the interaction produces secondary waves. Both the primary and secondary waves are observed at mesospheric heights. The validity of the nonlinear interaction was shown by the relationship between the frequencies and zonal wavenumbers of the waves involved in this interaction. The time intervals of wave persistence have been taken into account as well. The proposed approach is well supported by the experimental data.

There are some peculiarities in the interpretation of the EP flux convergence and divergence. The analyzed experimental data correspond mainly to the stage of the wave evolution when the largest amplitudes are observed and non-linear and dissipation terms are important. For the EP flux calculations we used wave parameters estimated for the whole month. Our numerical simulation (see Appendix) demonstrated that the calculated distribution of the regions of the largest EP flux divergence/convergence is similar to that when the linear theory is applicable, i.e. when divergence/convergence of the EP flux is in balance with a growth of the wave amplitudes; and we can use, for example, the data for an entire month.

3. Results

The MR data are given at several altitudes. Keeping this in mind we show the results of the SABER data analysis mainly in geometric coordinates. However the quasigeostrophic theory of the instability is simpler when the pressure is used as a vertical coordinate. Therefore the corresponding distributions are presented in log-pressure coordinates. It is well known that the log-pressure vertical coordinate taken as $7\log(P_0/\text{pressure})$ is close to the geometric height in the stratosphere and mesosphere. The perturbations of geopotential play the same role in the log-pressure coordinates as the ratio of pressure perturbations to ρ_0 (pressure/ρ_0. where ρ_0 is a zonal mean background density) in the geometric coordinates and their distributions are similar. We hope in this way that the using of different coordinates does not create problems with the interpretation.

3.1. Meridional wind measured by the meteor radar and obtained from the SABER data in February 2004

The results presented by Nozawa et al. (2003) and Merzlyakov et al. (2005) showed that the QTDW has the largest amplitudes at lower height levels available from the radar measurements. This is a reason mainly the 81-km height level is considered in this study for the Esrange radar. The wavelet spectrum calculated for the meridional wind oscillations measured at Esrange during February 2004 is shown in Fig. 1 (upper left plot). The spectral content calculated by the periodogram method for a period range from 1.5 days to 4.5 days is also shown in Fig. 1 (upper right plot). Three dominant peaks with periods of about 42-48 hours, 64 hours and 85 hours can be distinguished in both spectra. The second peak is dominant through the entire height interval of the radar measurements (not shown). We also present the results of wavelet and periodogram analysis applied to the meridional wind oscillations calculated from the SABER measurements (Fig. 1, lower two plots). The results were obtained for latitude of 67.5^0N and a height of 80 km by averaging winds calculated for latitudes 65^0 and 70^0N.

There is a good correspondence of the spectral peaks and their timing for both the radar and SABER data during the considered time interval (Fig.1). The amplitudes of wind oscillations estimated from the SABER dataset are weaker than their counterparts measured at Esrange. This is a result of averaging over a 10-degree latitudinal interval, because the theoretical and experimental investigations indicate a strong latitudinal dependence of the waves studied in this and other works (Hartmann, 1983; Lawrence and Randel, 1996). One has to take into account the difference in the sensitivity and the volume sampling of the instruments as well as any shortcomings of our assumptions when calculating wind velocity.

Finally, we conclude that the wind oscillations determined from the SABER data give a proper representation of the wind oscillations directly observed by the radar. This comparison defines a basis for analyzing sources and parameters of the prevailing oscillations in wind, pressure and temperature using only the global SABER data.

3.2. Eastward propagating waves as observed by SABER during February 2004

From the satellite data we can determine a set of zonal harmonics for each spectral component found in the periodogram plots (Fig. 1, right column of plots). Namely, the spectral component with a period of about 2 days (Fig. 2) corresponds mainly to eastward propagating oscillations with zonal wavenumbers 2 and 3. Two other peaks (64-hour and 84-hour) correspond mainly to oscillations propagating eastward with zonal wavenumber 1. Strong oscillations with periods of ~2-days can be distinguished near day 47. These oscillations, however, being with different wavenumbers suppress each other in the MR sounding region because of near opposite phases at the considered heights. Therefore we do not consider them in detail.

According to the quasi-geostrophic theory the change of the sign of the meridional gradient of the zonal mean quasi-geostrophic potential vorticity (Q_y) in a region is a necessary condition for the instability in this region. In the stratosphere and mesosphere the sign of Q_y is mainly positive. Therefore searching for the regions where $Q_y<0$ is equivalent to searching for the regions where Q_y changes its sign.Fig.3 presents distributions of the zonal mean zonal wind and Q_y for the first half of February 2004. Units of Q_y are Ω/R_e, where Ω is the Earth's rotation rate, R_e is the Earth's radius. The errors for the calculated zonal mean zonal wind grow from about 6% at 45^0N to 10% at 75^0N. The calculation of Q_y is equivalent to an estimation of the third derivative of the geopotential. Hence, the errors would be large and that is why we perform a smoothing of the Q_y distribution by using a triangle filter (0.25, 0.5, and 0.25). In this way the values of Q_y are presented with an error of about 30%. Fig.3 indicates that a strong polar jet was developed, and potentially unstable regions appeared in the first half of February 2004. In order to have confidence that the investigated oscillations can be generated in these regions we took into account results of numerical simulations (for example, Pfister, 1985; Salby, 2001; and see also Appendix). These results demonstrated that the critical line of the growing wave has a part placed in the region of $Q_y<0$. In Fig.3 the solid line

shows a critical line for the 2-day zonal wavenumber 2 oscillations. This line crosses the region of negative Q_y.

The dominant pressure and temperature oscillations of wave periods studied in this work are connected with eastward propagating waves of zonal wavenumbers 1 and 2 and with periods of 4-5-days, and about 2-days, respectively, during the first half of February 2004. The height-latitude distributions of perturbation amplitudes in meridional wind and temperature due to these waves are shown in Fig.4 (for the 4-day wave in Fig.4a and for the 2-day wave in Fig.4b). The coherence distributions calculated for pressure oscillations are also shown. The location of the maximum pressure amplitude is taken as a reference point. The divergence of the EP flux for these waves is presented in Fig.4 as well (bottom right plot). To estimate the errors of the EP flux divergence for the oscillations studied we calculated div (EP) for all spectral peaks corresponding to eastward propagating oscillations with periods ranging from 1.5 to 5 days and zonal wavenumbers from 1 to 3 (for a total of 45 spectral peaks). For each zonal wavenumber separately and for all peaks the r.m.s. error is about 0.25 m/s/day.

Figs. 3 and 4 reveal that the areas of the positive divergence and of the negative Q_y are overlapped (these areas occupy a common region). The positive and negative regions of the EP divergence are distributed in such a way that the corresponding zonal forcing acts to remove regions of the negative Q_y. The characteristic features of such unstable waves are: an equatorward momentum flux for waves on the equatorial flank of the jet and an opposite momentum flux for waves on the polar flank as well (Hartmann, 1983). These results give evidence for the jet instability as a source for the 2-day and 4-day waves. The EP fluxes are mainly downward directed (including regions with $Q_y > 0$) for both waves. It can be seen that the waves are forced at the equatorial flank of the jet. The instability appears due to a double jet structure, which is a characteristic feature of the zonal mean zonal wind distribution in winter of the Southern hemisphere and frequently observed in the Northern hemisphere (Manney and Randel, 1993). The maxima of the zonal mean zonal wind acceleration have values about -1m/s/day. Note that this value is the monthly mean for a single spectral component. Hence, the investigated waves exert a significant influence on the circulation in the upper stratosphere.

The 4-5-day wave has small amplitude of wind oscillations at 80 km height. Instead of this wave we found an oscillation with a period of 3-3.5 days. This oscillation is also an eastward propagating wave with zonal wavenumber 1. The distributions of wave amplitudes in pressure, temperature and the meridional wind component and the EP flux divergence for the 3-day wave are shown in Fig.5. Fig. 6 presents a possible generation mechanism of this 3-day oscillation by a nonlinear wave-wave interaction. The waves are shown in this figure at heights where the largest amplitudes are observed. Then the 3-3.5 day wave could be a difference secondary wave produced by the nonlinear wave-wave interaction between the 1.75-day s=2 wave and the 4-day s=1 wave. The validity of the zonal wavenumber and frequency relationships between the primary and the secondary waves gives strong evidence that the non-linear interaction really takes place. The magnitude of the maximum divergence of the EP flux for the 3-day wave is about one order of magnitude weaker than the corresponding values for the 2-day and 4-5-day waves. The same feature was obtained in our numerical simulations (see Appendix). The wavelet spectra presented in Fig. 6 show that all three waves appear simultaneously, and one needs to take into account their superposition. The 3-day wave exists during a burst of the 2-day wave activity. According to the theory (for example, Vanneste, 1995, paragraph 5) the 2-day wave is the main source of energy for the 3-day wave. The critical line of the 3-day wave only touches the region with the negative Q_y (see Fig. 3, the dashed line in the right plot).

The 2-day wind oscillations observed at a height of 80 km are a superposition of two spectral components of zonal wavenumbers 2 and 3. The second one is proposed to be a result of the nonlinear interaction between the s=2 primary wave of a 2-day period and a stationary planetary wave of zonal wavenumber 1 (SPW1), observed in February 2004 (Garcia et al., 2005). The EP flux divergence of the 2-day secondary wave is significantly smaller than the corresponding value of the

primary 2-day wave (not shown). A wave-1 counterpart of the 2-day wave is generated as well. Due to larger phase velocity it occupies a larger atmospheric region in height and latitude than wave 3, which is concentrated near its critical line and therefore becomes most prominent at 80 km.

The strongest spectral peak of the wind oscillations shown in Fig.2 is the peak of about 64-hour period. At 80 km, this peak seems to be a superposition of oscillations having zonal wavenumbers 1 and 3. We were not able to find coherent pressure oscillations for wave 3 at this height, so, most probably this spectral component is related to a noise spectrum. The height-latitude distributions of the perturbation amplitudes in meridional wind and in temperature for the 64-hour s=1 spectral component are presented in Fig.7. Additionally, the coherence distribution for pressure oscillations and divergence of the EP flux are shown as well. One can see that this oscillation is observed mainly in the mesosphere. Figures 7-8 give evidence for the generation of this oscillation by the jet instability on the polar flank of the jet (at its top). Again the regions of the EP flux divergence and convergence of the oscillation are distributed in such a way to remove conditions for the jet instability. The EP flux is mainly downward directed, and this means a dynamical influence on the lower layers. However, this influence is significantly weaker than that of the 4-day and 2-day waves considered above.

3.3. Eastward propagating waves during February 2003

Here we present some results for February 2003. During this month the polar night jet was weaker than the jet during February 2004. Thus we have opportunity to compare the QTDW activity for different background conditions and to indicate that the QTDW activity really depends on the polar jet strength. In Fig. 9 the upper plots show the background zonal mean zonal wind and the meridional gradient of Q_y. As it can be seen the polar jets are very different in Februaries of 2003 and 2004. The jet of February 2003 is wider and located farther from the North Pole than the jet in February 2004. As a consequence of this we can find a region with strong negative gradient Q_y at the polar flank of the jet. The magnitude of the negative Q_y is significantly smaller than that for February 2004. As a result the eastward propagating perturbations in wind and temperature are weaker in February 2003 than those in February 2004. Again, as in February 2004 we obtained a good correspondence between the meridional wind oscillations observed by the MR at Esrange and those calculated from the SABER measurements (Fig.9, bottom plots).

4. Conclusions

We analyzed pressure and temperature data obtained by the SABER instrument on board the TIMED satellite during February 2003 and 2004. The wind oscillations were estimated from the pressure oscillations under a few assumptions: no vertical wind, no diffusion, and no non-linear terms. We employed a simple nonlinear model of wave propagation through a non-uniform atmosphere to check the assumptions. The numerical results gave us a basis for employing our approach in order to estimate the winds in cases when a given wave is generated by the jet instability or by nonlinear wave-wave interaction. In its turn this gave a possibility to calculate the EP flux, the divergence of the EP flux and to analyze the sources of the observed atmospheric oscillations and their influence on the background atmosphere. In experimental studies usually only the period when the waves reach the largest amplitudes is analyzed. In this study we estimated wave parameters for the entire month. During this period the waves generated by the instability appear and disappear. If we take the wave activity equation (Andrews, 1987) and average it over this time period we obtain the average positive EP-flux divergence and the zero term with the time derivative. This positive divergence is balanced by external sinks and sources of the wave (the left part of the equation). Thus, during this period the average divergence is mainly in balance with the friction (if it is significant) and with the nonlinear terms. Our numerical results showed that the distribution of the regions of the largest EP flux divergence/convergence calculated in such a way is

very similar to that for a stage when the wave's growth is balanced by the divergence of the EP flux. Our numerical simulation also revealed the instability of the polar night jet tuned to be similar with that observed in February 2004. On the other hand, the nonlinearity was a weak source for waves in comparison with the instability. This is a reason the instability to be accepted as a source of the primary waves.

Briefly the results of our analysis could be summarized as follows:

– We have demonstrated a good correspondence between the meridional winds measured by the meteor radar at Esrange and those retrieved from the pressure oscillations measured by the SABER instrument.

– Significant pressure, temperature and wind oscillations with periods of 1.5-5 days were found to propagate eastward in the upper middle atmosphere of the Northern hemisphere during the winter of 2004.

– The appearance of these waves at mesospheric heights could be explained as products of the polar jet instability and nonlinear wave-wave interactions.

– These waves occupy a region from the upper stratosphere up to the upper mesosphere providing coupling of these layers. The vertical components of the EP flux for these waves are mainly downward directed. This suggests a dynamical influence of the mesosphere on the upper stratosphere.

Pursuing our main goal to correlate the SABER and MR observations of atmospheric perturbations at a particular range of periods we left some interesting features unstudied. For example, a ~10-day zonally symmetric oscillation was observed in February 2004. The maximum amplitude averaged over the entire month was ~10 m/s at 55^0N and 50 km height. This oscillation periodically changed the jet strength and this possibly led to appearance of the periodical bursts of the 2-day wave activity during this month.

Appendix

Numerical simulations are based on the 3D nonlinear time dependent model describing the wave propagation in a non-uniform atmosphere (for details and references see Merzlyakov and Jacobi, 2004). Briefly, this model employs a finite-difference approach in latitude and height directions with steps of 3^0 and 0.25H, respectively (H is a scale height of the uniform atmosphere, taken as 7 km), and the spectral expansions in longitude. All variables are expanded in zonal harmonics ranging from -6 to 6. The model solves the governing primitive equations in log-pressure coordinates. It extends from 10^3 hPa (the model bottom) through the lower thermosphere ($2.8*10^{-5}$ hPa). Small-scale mixing by unresolved gravity waves is represented as turbulent diffusion. The gravity wave – mean flow interaction is approximated as a body force. Thus, the model does not reproduce the interaction between gravity and planetary waves. The molecular and eddy viscosity and thermal conductivity, Newtonian cooling, ion drag are taken into account.

A reference temperature distribution was constructed by merging the temperature distribution from the climatological model by Fleming et al. (1988) and the zonal mean temperature distribution calculated from the SABER measurements for February 2004. At the boundaries of the SABER temperature distribution an interpolation was applied. The above described procedure smoothes the zonal mean temperature distribution for February 2004 and lead to a smoothed zonal mean zonal wind distribution. To obtain a background wind distribution close to the real one the winter polar jet was accelerated till the maximum speed of 104 m/s.

The numerical run includes a few steps: we set up zonally symmetric initial conditions with zero wind and a model run was carried until a steady state, then a seed of noise was introduced in the model, and the simulation is performed for a month. The noise level is small and the results do not

depend on that level and on the time spectrum of the noise. Under the obtained background conditions (see Fig.10) we observed a growth of the 90-hour wave due to the jet instability in the winter hemisphere. The wave propagated eastward with zonal wavenumber 2. A widely accepted concept which is based on the linear theory of wave propagation in the atmosphere without dissipation (Andrews, 1987) is that a region of positive divergence of the EP flux corresponds to a growth of wave amplitude when the meridional gradient of the quasigeostrophic potential vorticity (Q_y) is negative in that region. When the time interval with the large wave amplitude is selected, we have to take into account the dissipation and nonlinear terms to balance the EP flux divergence. This follows from the wave activity equation (Andrews, 1987). When averaging over the time interval with large wave amplitude, the time derivative term is close to zero. In the same time we obtain the large positive divergence of the EP flux. This term has to be balanced by external sources and sinks. In our case these sinks are nonlinear terms and dissipation. The importance of the nonlinear terms in the wave balance equation was demonstrated, for example, by Prata (1984). Fortunately, the results of the numerical simulations (not shown) give the same locations of regions with negative and positive EP divergence for both linear and nonlinear stages of the wave evolution.

Using the output fields of velocities, pressure and temperature and the linear balance equations for retrieving of wind perturbations from pressure oscillations we tested the assumptions adopted in this study. In Fig. 10 the true and approximated (retrieved) wind distributions are presented. The divergence of the EP flux is also shown. The approximated value was calculated in the same way as in the experimental data analysis. Both wind components were retrieved with errors less than 2%. The retrieved distribution of the divergence of the EP flux shows correct locations and gives the proper order of magnitude of the maximum negative and positive divergence of the true EP flux.

The simulation of the nonlinear interaction between the 4-day s=1wave and the 2-day s=2 wave was carried out for a stable background wind distribution. These primary waves were generated by thermal sources and had amplitudes of the same order as observed by the SABER instrument. We obtained that the nonlinear interaction between the given waves can really generate the s=1 wave of observed amplitudes with a period of 3 days. The divergence of the EP flux for secondary waves was found to be a few times smaller (on about one order) than the divergence of the primary waves. The procedure of the wind retrieval from the pressure oscillations for the secondary wave was also tested. The errors of the retrieval (not shown) were close to those presented for the unstable atmosphere, except for the error for the zonal wind component which was about 6% at high latitudes. The last can be anticipated because the non-linear terms work mainly in the momentum equation for the zonal wind component.

Thus we obtained that both wind components are retrieved with errors of a few percents in the framework of our numerical approach. For the meridional component the error is less than 2%. Retrieved EP flux distributions correctly represent true EP flux distributions for the largest magnitude of the divergence. Regarding the SABER data analysis, it is worth noting that our numerical simulation does not provide a stringent test of the analysis method because only part of the real atmospheric variability was taken into account.

Acknowledgements

We are grateful to the SABER team for the access to the SABER instrument data. This work was supported in part by the NASA TIMED Program under grant NAG5-5028 to the University of Colorado and subcontract to the Institute for Experimental Meteorology. We are deeply indebted to the reviewers for their valuable corrections and comments.

REFERENCES

Andrews, D.G. On the interpretation of the Eliassen-Palm flux divergence, Quarterly Journal of Royal Meteorological Society, 113, 323-338, 1987.

Allen, D.R., Stanford, J.L., Elson, L.S., Fishbein, E.F., Froidevaux, L., and J.W. Waters, The 4-day wave in the stratosphere and mesosphere as observed from the Upper Atmosphere Research Satellite Microwave Limb Sounder, Journal of the Atmospheric Sciences, 54, 420-434, 1997.

Coy, L., Stajner, I., DaSilva, A. M., Joiner, J., R. B. Rood, S. Pawson, and S. J. Lin, High-frequency planetary waves in the polar middle atmosphere as seen in a data assimilation system, Journal of the Atmospheric Sciences, 60, 2975-2992, 2003.

Fleming E.L., S. Chandra, M.R. Shoerberl, and J.J. Barnett, Monthly mean global climatology of temperature, wind, geopotential height, and pressure for 0-120 km, NASA Tech. Memorandum, 100697, 85 pp., 1988.

Garcia, R. R., Lieberman, R., Ruassell III, J.M., Mlynczak, M.G., Large-Scale Waves in the Mesosphere and Lower Thermosphere Observed by SABER, Journal of the Atmospheric Sciences, 62, 4384-4399, 2005.

Hartmann, D.L., Barotropic instability of the polar night jet stream, Journal of the Atmospheric Sciences, 40, 817-835, 1983.

Holton, J.R., The dynamic meteorology of the stratosphere and mesosphere, Meteorological monographs, 18, 1975.

Lait, L.R. and Stanford, J.L., Applications of asynoptic space-time Fourier transform methods to scanning satellite measurements, Journal of the Atmospheric Sciences, 45, 3784-3809, 1988.

Lawrence, B.N., Fraser, G.J., Vincent, R.A. and A. Phillips, The 4-day wave in the Antarctic mesosphere, Journal of Geophysical Research, 100, 18899-18908, 1995.

Lawrence, B.N., Randel, W.J., Variability in the mesosphere observed by the Nimbus 6 PMR, Journal of Geophysical Research, 101, 23475-23490, 1996.

Manney, G.I. and Randel, W.J., Instability at the winter stratopause: a mechanism for the four day wave, Journal of the Atmospheric Sciences, 50, 3928-3938, 1993.

Manney, G.L., K. Krüger, J. L. Sabutis, S.A. Sena, and S. Pawson, The remarkable 2003-2004 winter and other recent warm winters in the Arctic stratosphere since the late 1990s, Journal of Geophysical Research, 110, D04107, doi:10.1029/2004JD005367, 2005.

Mechoso, C.R., Hartmann, D.L., An observational study of traveling planetary waves in the Southern Hemisphere, Journal of the Atmospheric Sciences, 39, 1921-1935, 1982.

Merzlyakov, E.G. and Ch. Jacobi, Ch., Quasi-two-day wave in an unstable summer atmosphere – some numerical results on excitation and propagation, Annales Geophysicae, 22, 1917-1929, 2004.

Merzlyakov E.G., Portnyagin Yu.I., Makarov N.A., Forbes J., Palo S., Eastward-Propagating Day-to-Day Wind Oscillations in the Northern Polar Mesosphere/Lower Thermosphere, Izvestiya, Atmospheric and Oceanic Physics 41, 72-84, 2005.

Nozawa S., Imaida S., Brekke A., Hall C.M., Manson A., Meek C., Oyama S., Dobashi K., and Fujii R., The quasi 2-day wave observed in the polar mesosphere, Journal of Geophysical Research, 108. No.D2. doi:10.1029/2002JD002440, 2003.

Pfister, L., Baroclinic instability of easterly jets with applications to the summer mesosphere. Journal of the Atmospheric Sciences, 42, 313–330, 1985.

Prata, A.J., The 4-day wave, Journal of the Atmospheric Sciences, 41, 150-155, 1984.

Russell, J. M. III, Mlynczak, M. G., Gordley, L. L., Tansock, J., and R. Esplin. An overview of the SABER experiment and preliminary calibration results, Proc. SPIE, 44th Annual Meeting, Denver, Colorado, July 18-23, Vol. 3756, 277-288, doi:10.1117/12.366382, 1999.

Salby, M.L., Sampling theory for asynoptic satellite observations. Part I: Space-time spectra, resolution, and aliasing, Journal of the Atmospheric Sciences, 39, 2577-2600, 1982.

Salby, M.L., Callaghan, P.F., Seasonal Amplification of the 2-Day Wave: Relationship between Normal Mode, and Instability, Journal of the Atmospheric Sciences, 58, 1858-1869, 2001.

Vanneste, J., Explosive resonant interaction of baroclinic Rossby waves and stability of multilayer quasi-geostrophic flow, Journal of Fluid Mechanics, 291, 83-107, 1995.
Venne, D.E. and Stanford, J.L., Observation of a 4-day temperature wave in the polar winter stratosphere, Journal of the Atmospheric Sciences, 36, 2016-2019, 1979.
Venne, D.E. and Stanford, J.L., An observational study of high-latitude stratospheric planetary waves in winter, Journal of the Atmospheric Sciences, 39, 1026-1034, 1982.

Figure captions

Fig.1: Amplitude (m/s) wavelet (left column of plots) and periodogram (right column of plots) spectra of oscillations in the meridional wind measured by the MR at Esrange (68^0N, 21^0E, 81 km) (upper row of plots) and calculated from the SABER data (67.5^0N, 21^0E, 80 km) (bottom row of plots).

Fig.2: Wavelet spectra of the eastward propagating oscillations in the meridional wind (m/s) with zonal wavenumbers from 1 to 3 (from top to bottom, correspondingly) at 67.5^0N.

Fig.3: Background atmosphere for the first half of February 2004: (left plot) the zonal mean zonal wind (m/s), (right plot) the meridional gradient of the quasi-geostrophic potential vorticity (units are Ω/R_e). The solid line is a critical line for the 2-day zonal wavenumber 2 oscillation; the dashed line is a critical line for the 3-day zonal wavenumber 1 oscillation.

Fig.4a: The 4-day s=1 eastward propagating spectral component in pressure (upper left plot, coherence is shown), in meridional wind (upper right plot) and in temperature (bottom left plot); the divergence of the EP flux for this wave is shown in the bottom right plot.

Fig.4b: The same as Fig. 4a but for the 1.7-day s=2 eastward propagating spectral component

Fig.5: The same as Fig. 4 but for the secondary 3-3.5 day m=1 eastward propagating spectral component.

Fig.6: A proposed mechanism of the 3-day s=1 wave (bottom plot) forcing by the nonlinear interaction between the primary 2-day s=2 wave (middle plot) and 4-day s=1 wave (upper plot).

Fig.7: The same as Fig. 4a but for the 64-hour s=1 eastward propagating spectral component

Fig.8: Background atmosphere for the second half of February 2004: (left plot) the zonal mean zonal wind (m/s), (right plot) the meridional gradient of the quasi-geostrophic potential vorticity (units are Ω/R_e). The solid line is a critical line for the 64-hour s=1 oscillation.

Fig.9: The zonal mean zonal wind (m/s) in February 2003 (top left plot) and meridional gradient of the zonal mean quasi-geostrophic potential vorticity (top right plot). Wavelet transformations of the meridional wind data calculated from the Saber pressure data (bottom left plot) and obtained by the MR at Esrange (bottom right plot).

Fig10: (a) Numerical results for the 90-h unstable wave: (top left plot) the background zonal mean zonal wind (m/s) and (top right plot) meridional gradient of the zonal mean quasi-geostrophic potential vorticity (in Ω/R_e); the regions of the negative gradient are shaded. The dashed line is the critical line.

(b) Comparison of the true (left column of plots) and retrieved (right column of plots) parameters of the 90-h unstable wave: (from the top) zonal wind U, meridional wind V, and divergence of the EP flux; values are given in relative units.

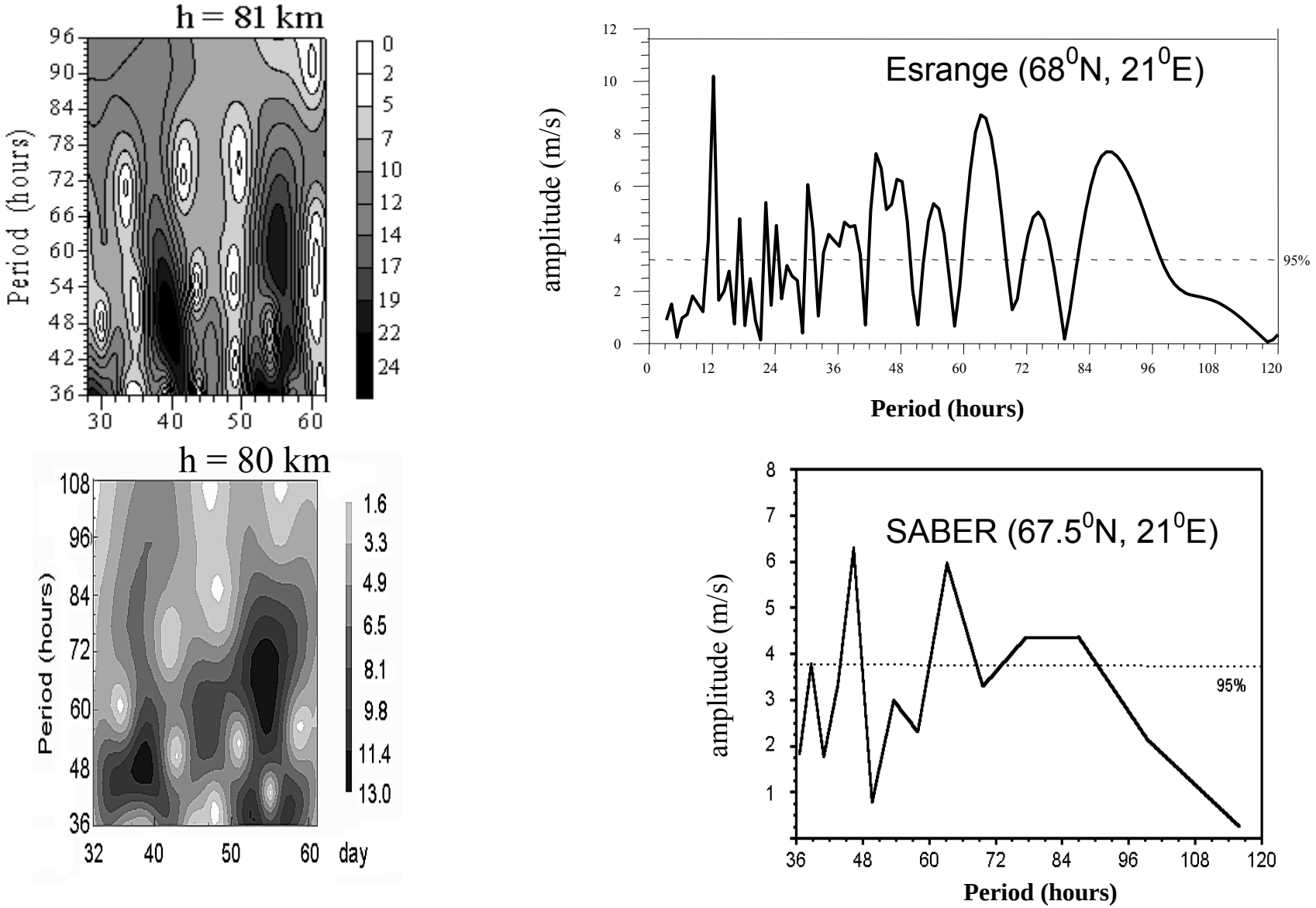

Fig.1: Amplitude (m/s) wavelet (left column of plots) and periodogram (right column of plots) spectra of oscillations in the meridional wind measured by the MR at Esrange (68^{0}N, 21^{0}E, 81 km) (upper row of plots) and calculated from the SABER data (67.5^{0}N, 21^{0}E, 80 km) (bottom row of plots).

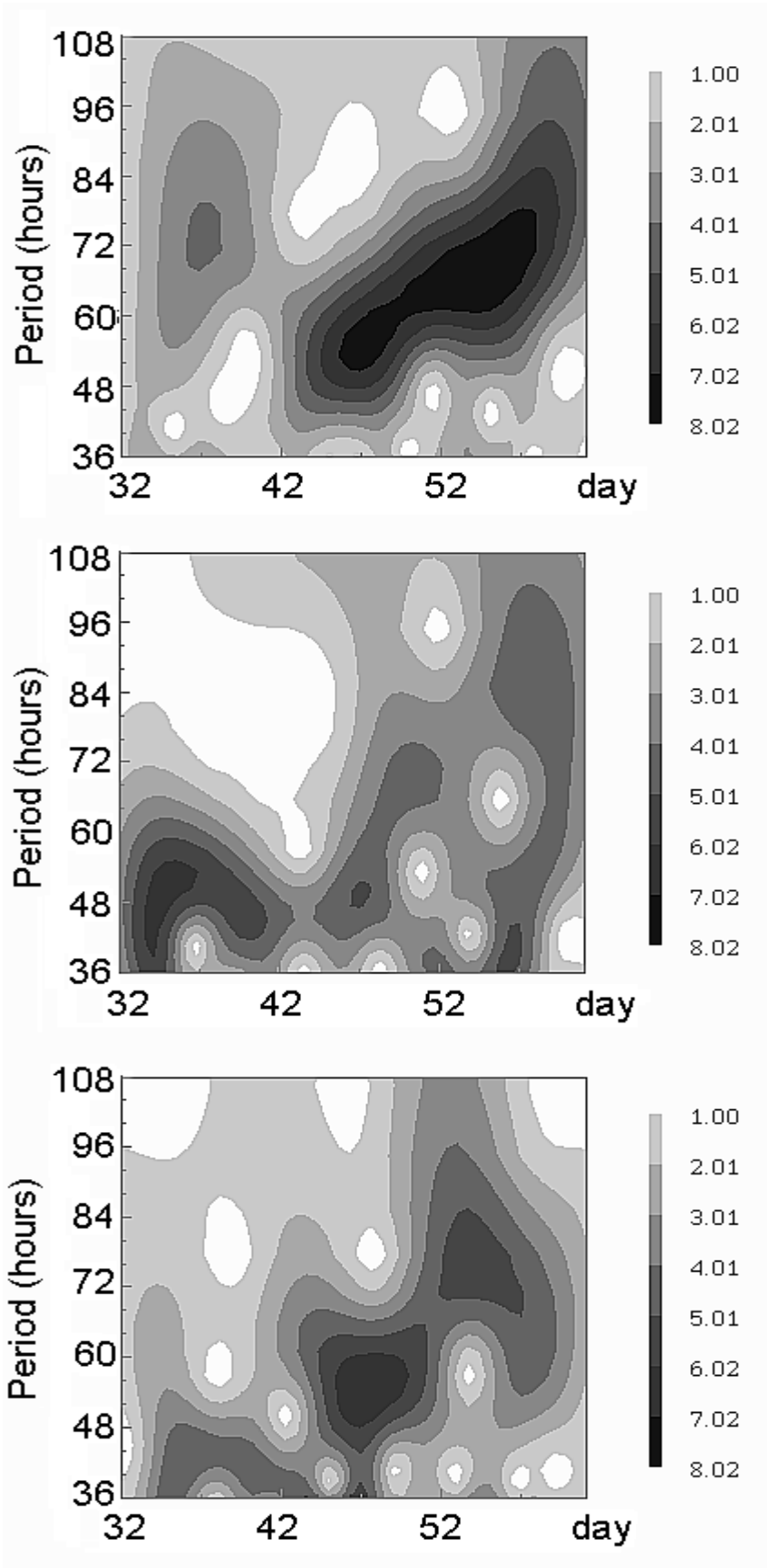

Fig.2: Wavelet spectra of the eastward propagating oscillations in the meridional wind (m/s) with zonal wavenumbers from 1 to 3 (from top to bottom, correspondingly) at 67.5^0N.

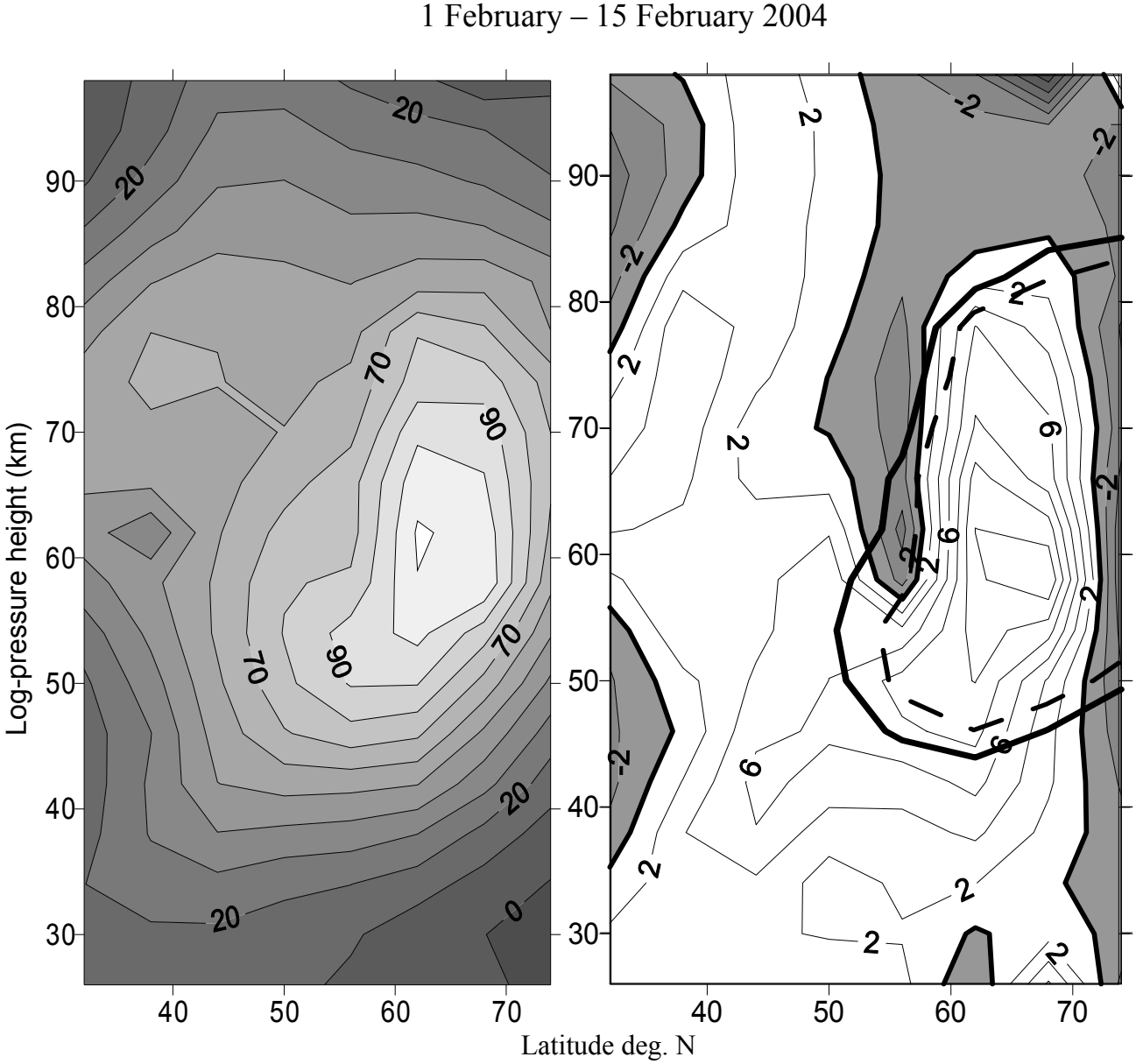

Fig.3: Background atmosphere for the first half of February 2004: (left plot) the zonal mean zonal wind (m/s), (right plot) the meridional gradient of the quasi-geostrophic potential vorticity (units are Ω/R_e). The solid line is a critical line for the 2-day zonal wavenumber 2 oscillation; the dashed line is a critical line for the 3-day zonal wavenumber 1 oscillation.

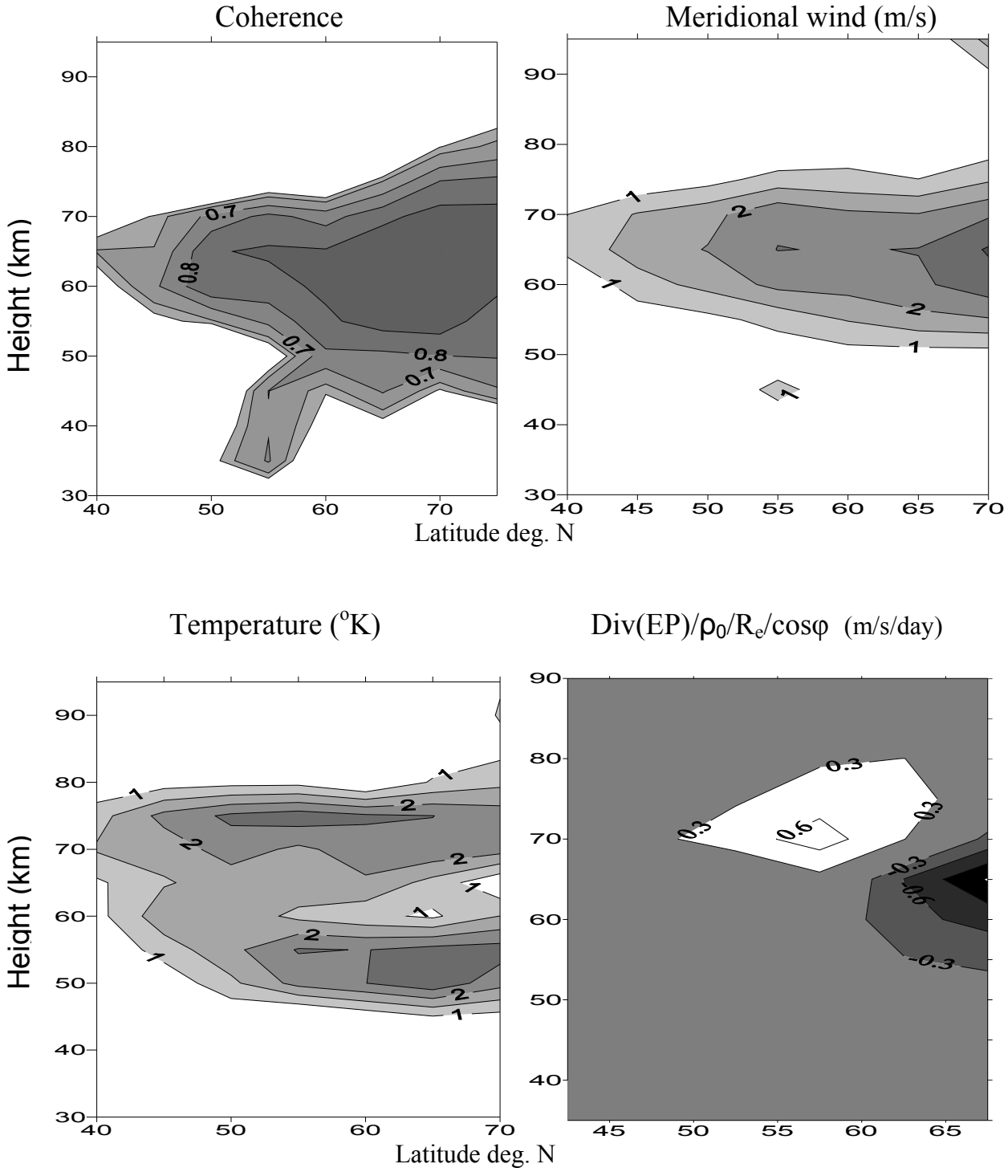

Fig.4a: The 4-day s=1 eastward propagating spectral component in pressure (upper left plot, coherence is shown), in meridional wind (upper right plot) and in temperature (bottom left plot); the divergence of the EP flux for this wave is shown in the bottom right plot.

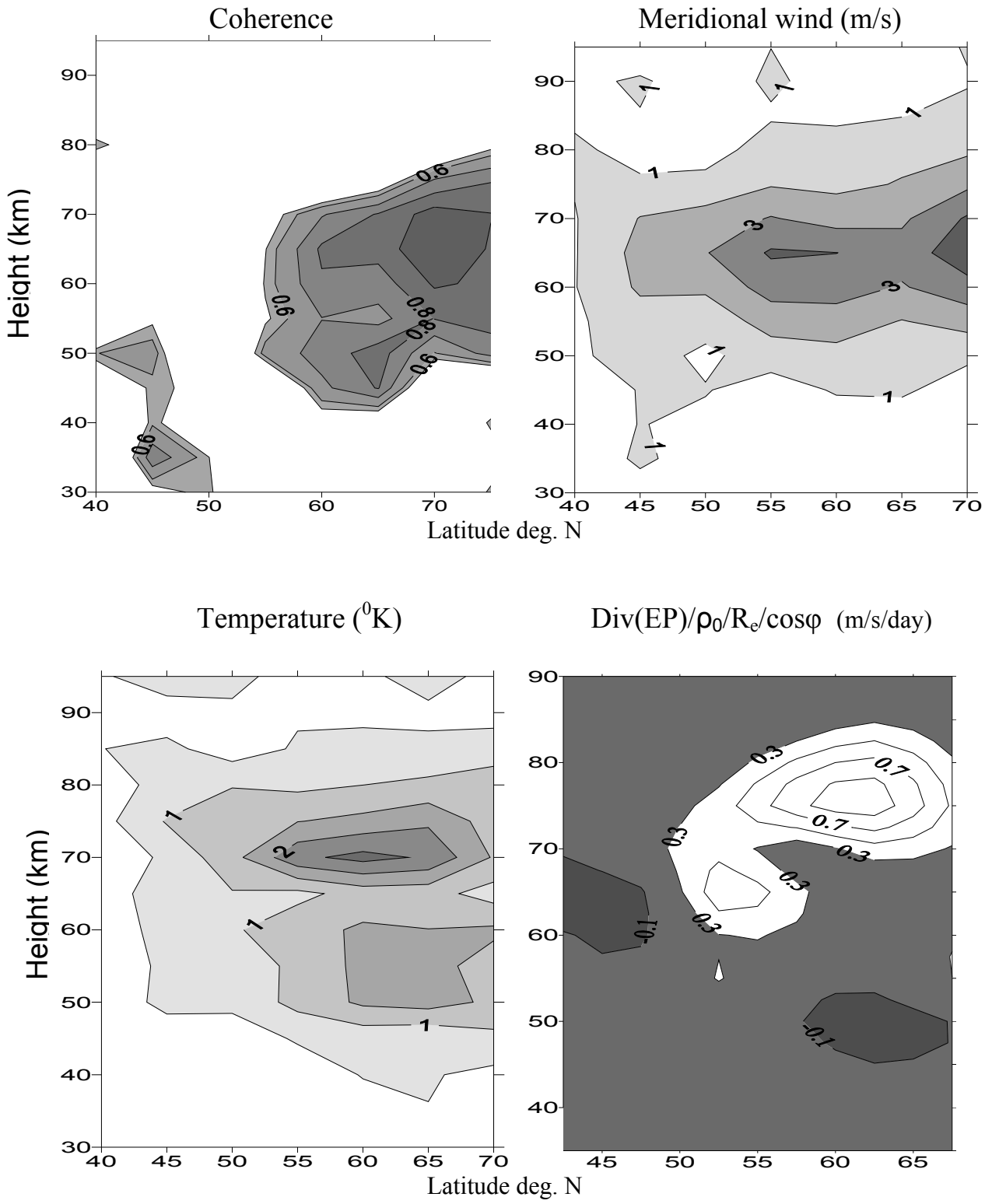

Fig.4b: The same as Fig. 4a but for the 1.7-day s=2, eastward propagating spectral component

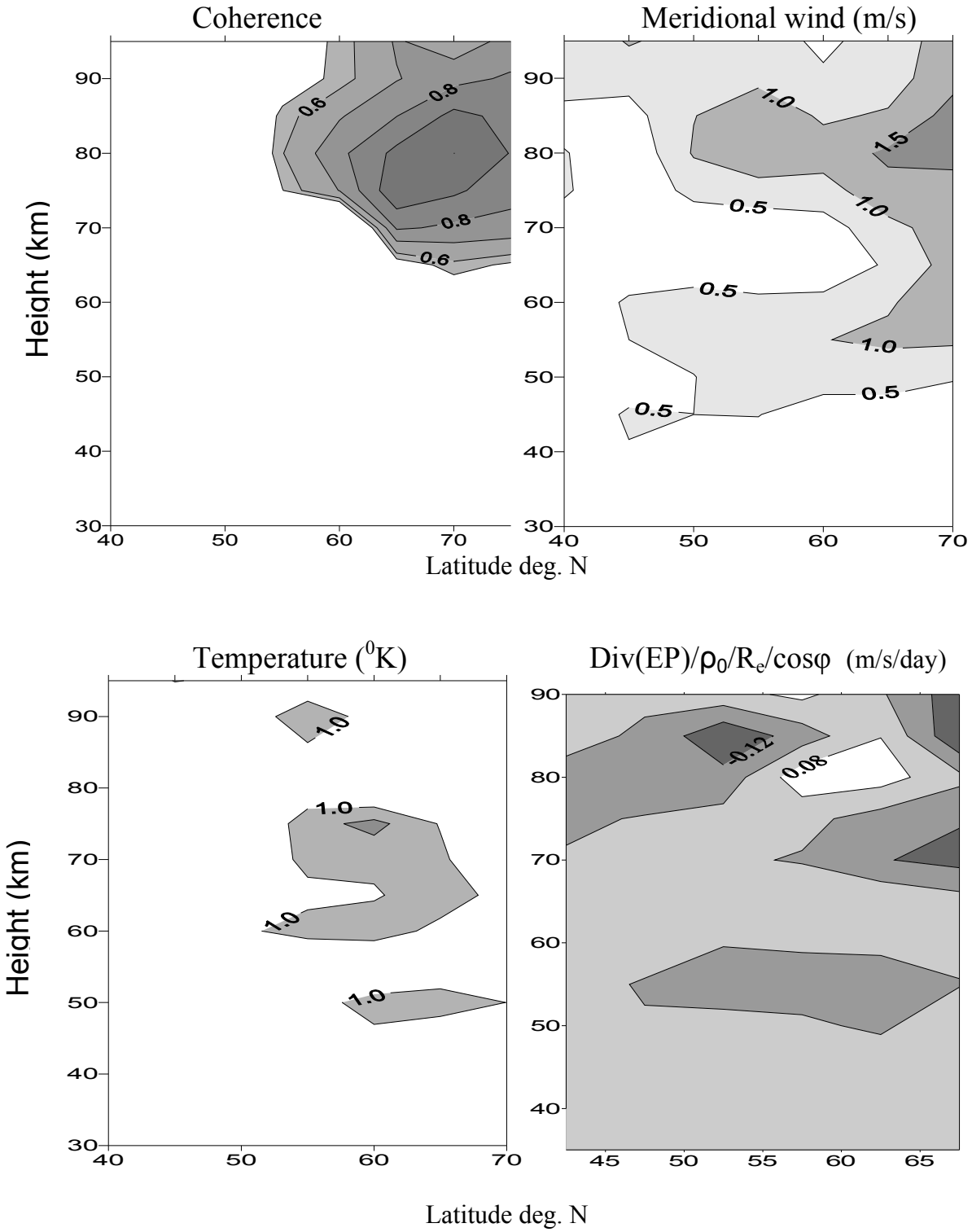

Fig.5: The same as Fig. 4 but for the secondary 3-3.5 day m=1 eastward propagating spectral component.

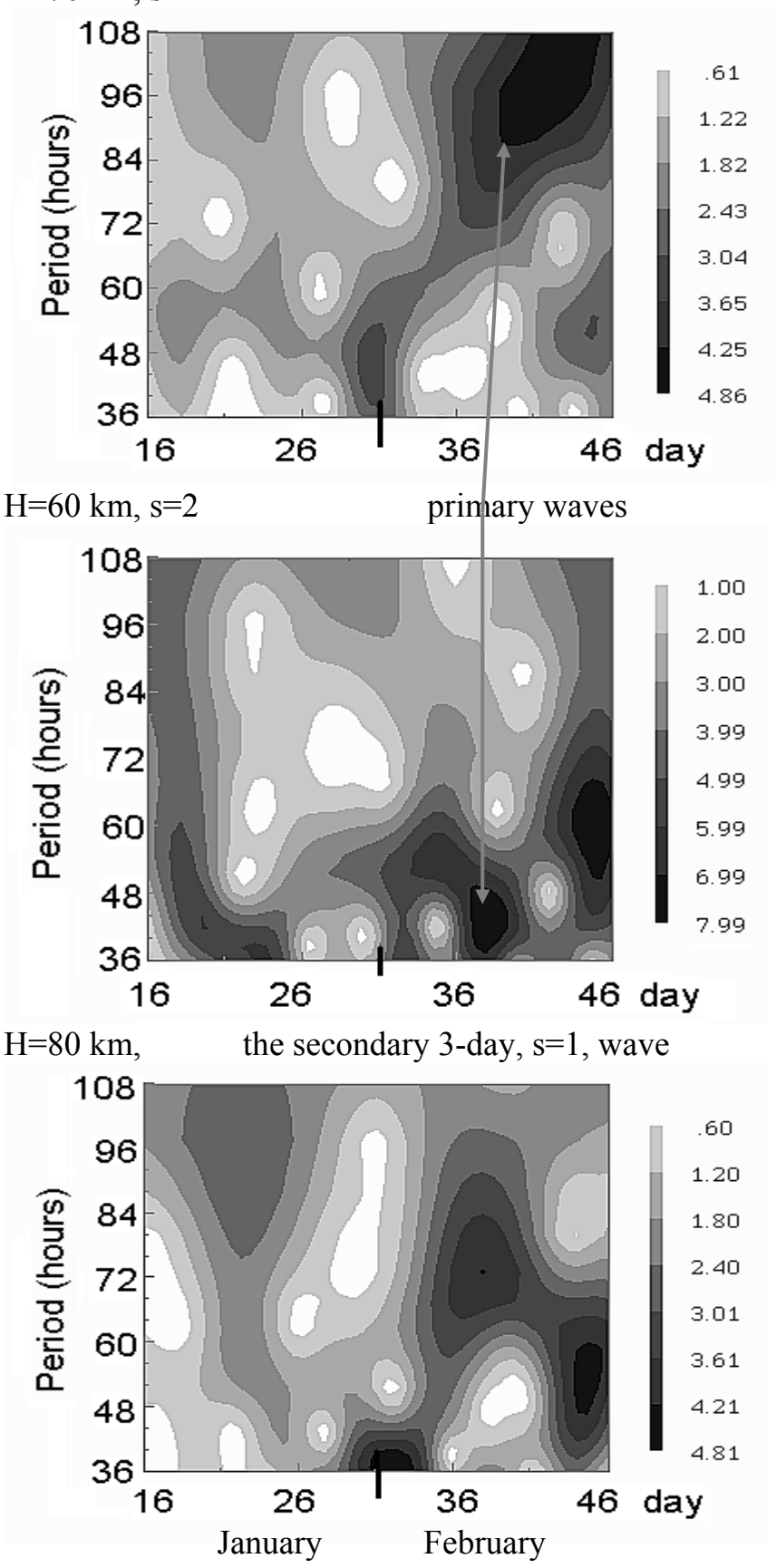

Fig.6: A proposed mechanism of the 3-day s=1 wave (bottom plot) forcing by the nonlinear interaction between the primary 2-day s=2 wave (middle plot) and 4-day s=1 wave (upper plot).

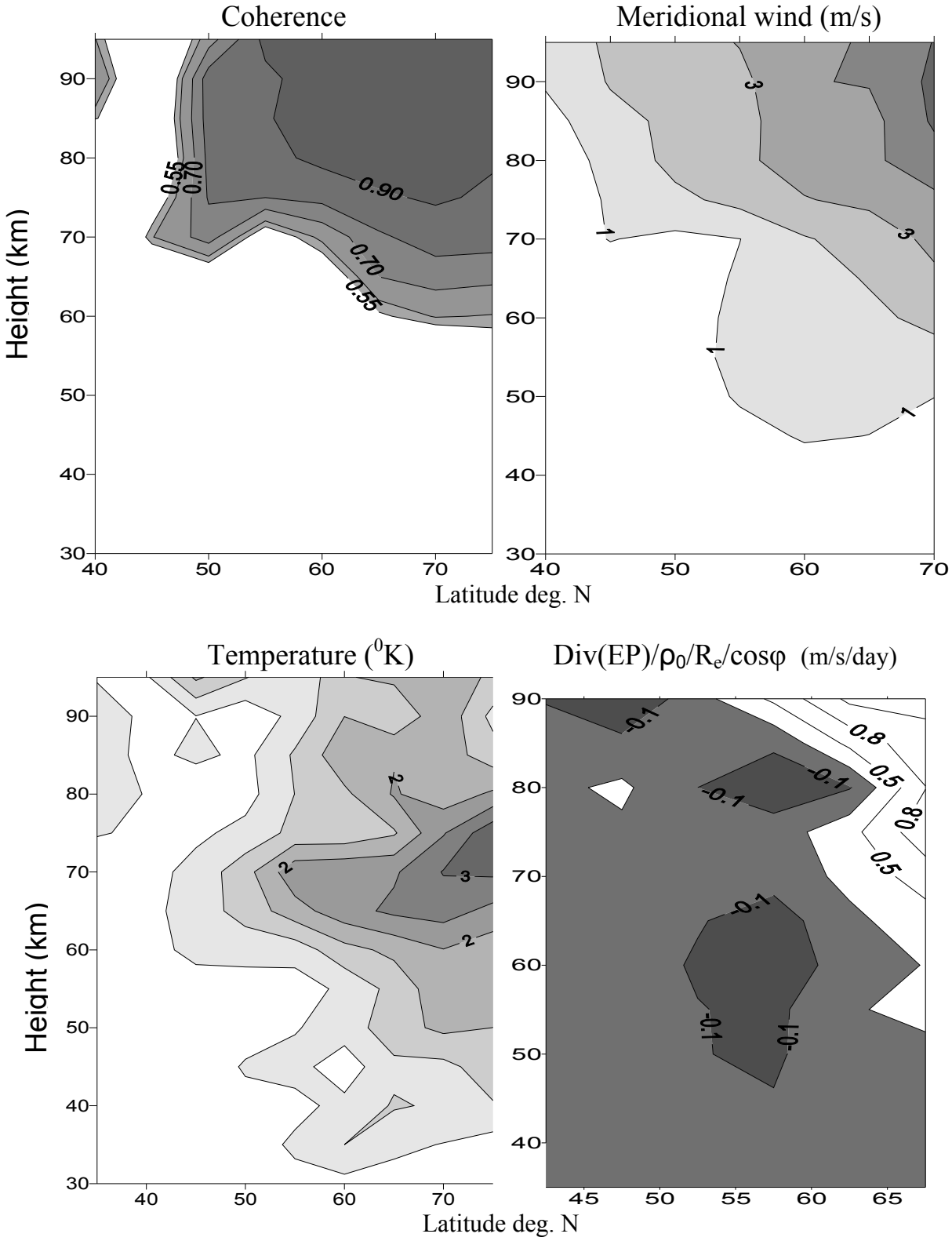

Fig.7: The same as Fig. 4a but for the 64-hour s=1 eastward propagating spectral component

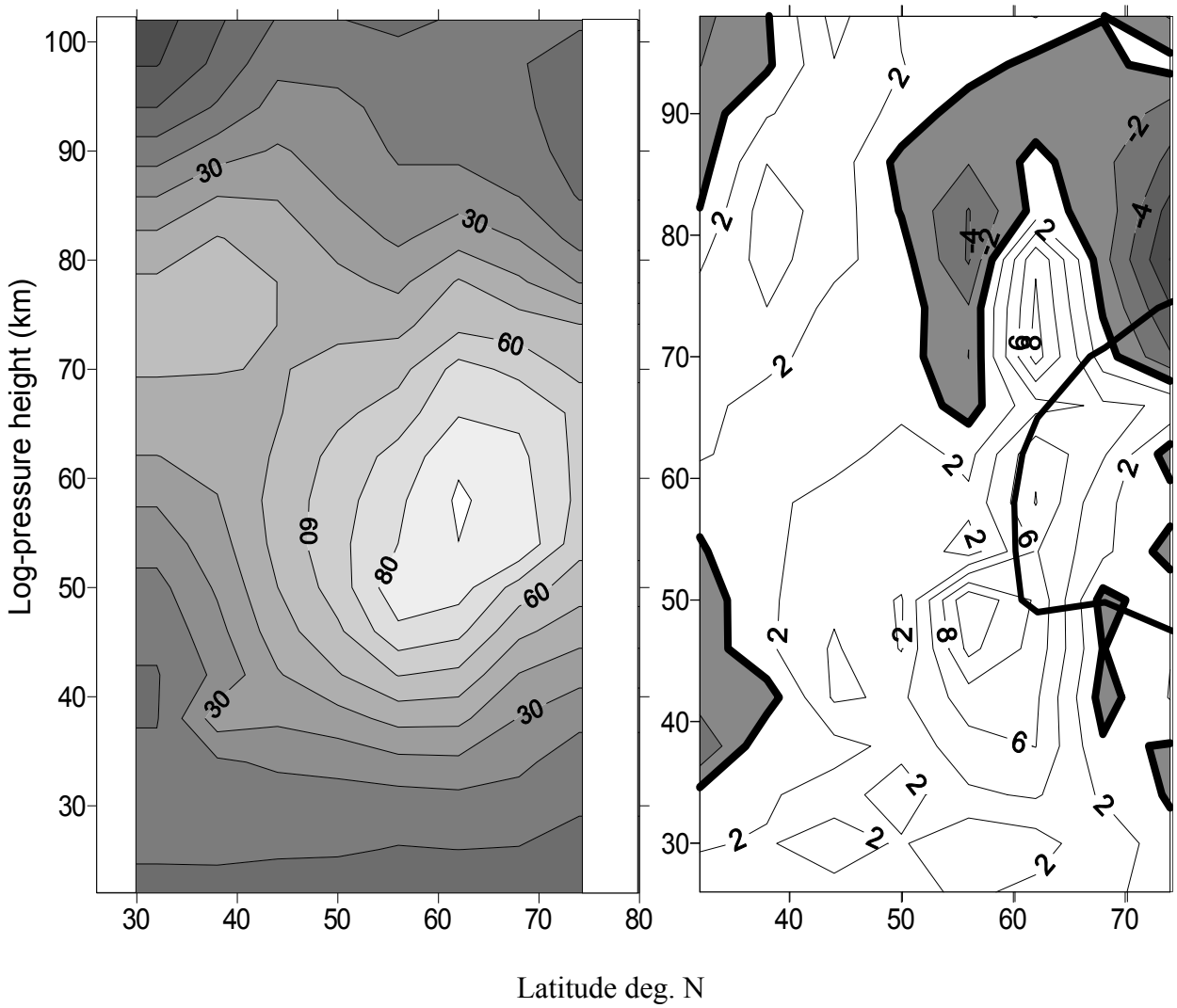

Fig.8: Background atmosphere for the second half of February 2004: (left plot) the zonal mean zonal wind (m/s), (right plot) the meridional gradient of the quasi-geostrophic potential vorticity (units are Ω/R_e). The solid line is a critical line for the 64-hour s=1 oscillation.

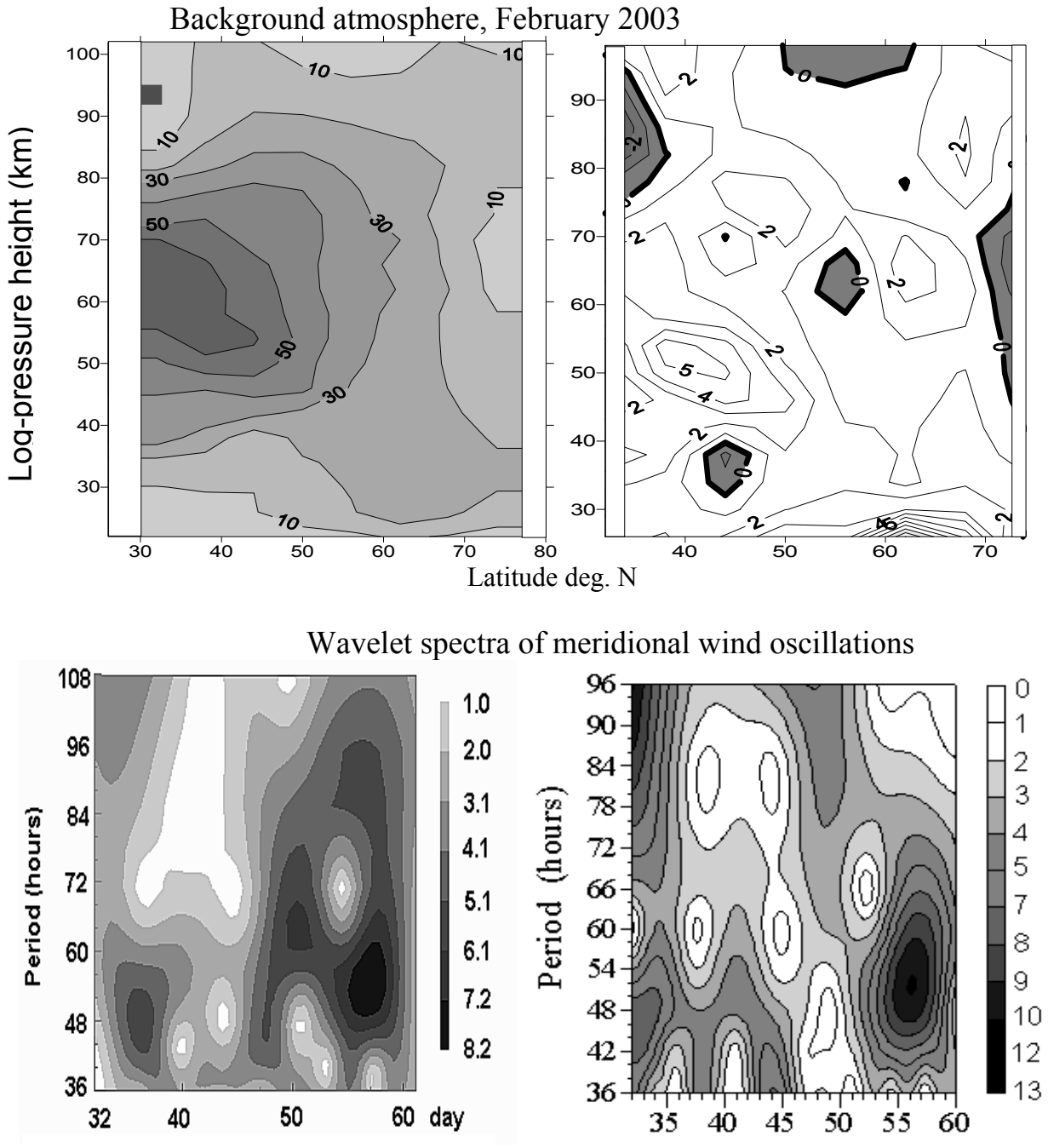

Fig.9: The zonal mean zonal wind (m/s) in February 2003 (top left plot) and meridional gradient of the zonal mean quasi-geostrophic potential vorticity (top right plot). Wavelet transformations of the meridional wind data calculated from the Saber pressure data (bottom left plot) and obtained by the MR at Esrange (bottom right plot).

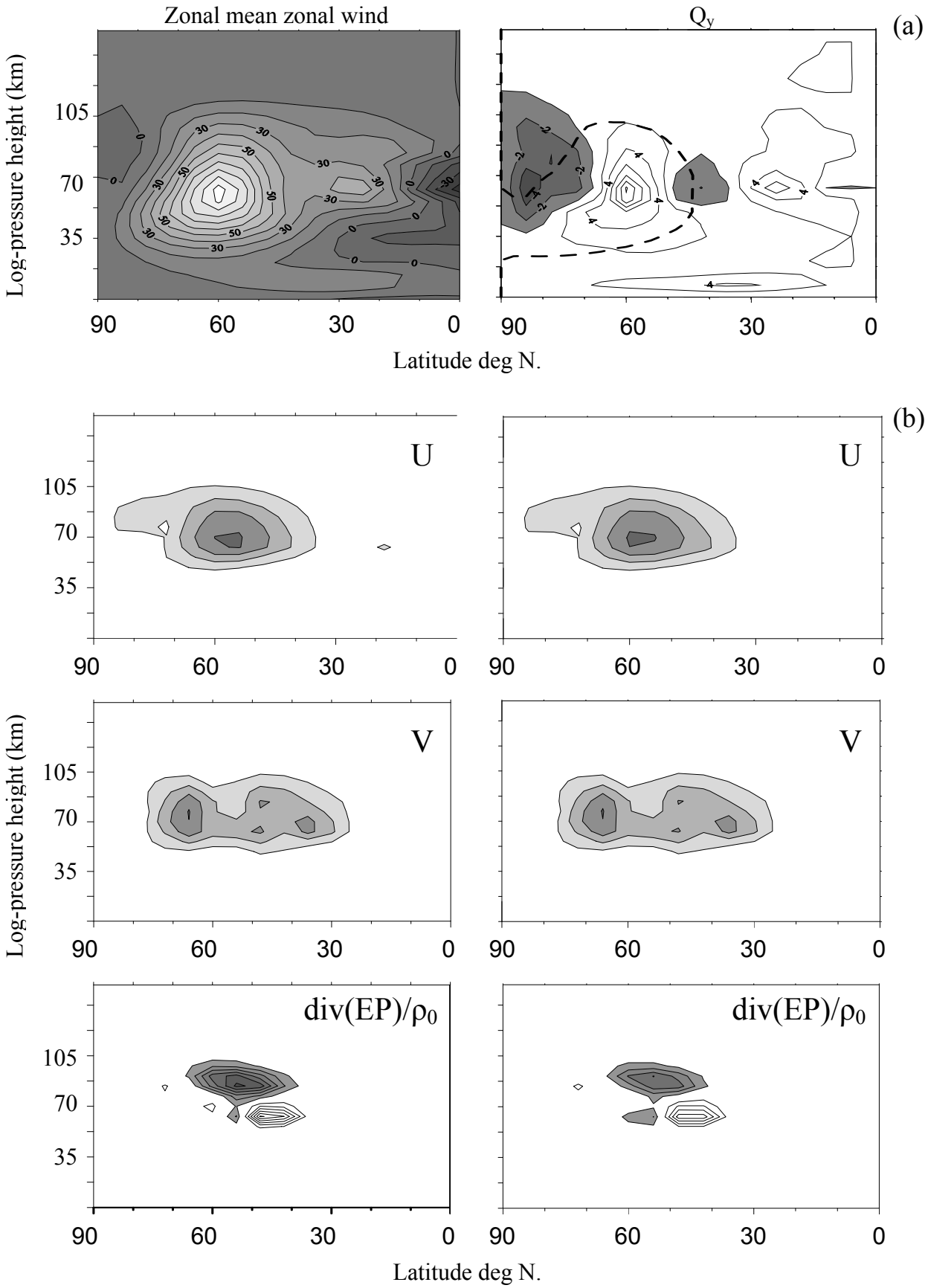

Fig10: (a) Numerical results for the 90-h unstable wave: (top left plot) the background zonal mean zonal wind (m/s) and (top right plot) meridional gradient of the zonal mean quasi-geostrophic potential vorticity (in Ω/R_e); the regions of the negative gradient are shaded. The dashed line is the critical line.

(b) Comparison of the true (left column of plots) and retrieved (right column of plots) parameters of the 90-h unstable wave: (from the top) zonal wind U, meridional wind V, and divergence of the EP flux; values are given in relative units.